Soft Matter

Cite this: *Soft Matter*, 2011, **7**, 10010

www.rsc.org/softmatter

PAPER

Morphology and organization of tissue cells in 3D microenvironment of monodisperse foam scaffolds†

Jing-ying Lin,[a] Wan-jung Lin,[b] Wei-hong Hong,[b] Wei-chun Hung,[c] Stephanie H. Nowotarski,[d] Susana Montenegro Gouveia,[e] Ines Cristo*[fg] and Keng-hui Lin*[ac]

Received 3rd March 2011, Accepted 4th August 2011
DOI: 10.1039/c1sm05371j

Here we demonstrate an efficient method to fabricate large-domain monodisperse foam scaffolds made of gelatin for 3D cell culture. We tested three distinct tissue cell types cultured in foam scaffolds composed of uniform spherical pores. The cells displayed appropriate morphological and physiological characteristics: epithelial cells formed cyst-like structures and were polarized inside pores, myoblasts adopted a tubular structure and fused into myotubes, and fibroblasts exhibited a wide variety of morphologies. Scaffolds with uniform pores can thus provide a platform for systematic study of 3D cell–matrix interactions.

Introduction

Recent research has revealed that the microenvironment around tissue cells influences behaviours such as drug responses,[1] differentiation,[2] and tissue morphogenesis.[3] In particular, the dimensionality of the microenvironment is an important factor; three-dimensional (3D) microenvironments mimic *in vivo* conditions and enable *in vitro* 3D tissue models.[4] Various fabrication processes and materials have been developed to create 3D microenvironments, especially in the field of tissue engineering. The typical 3D microenvironment for cells includes hydrogels such as collagen, matrigel, and fibrinogen, or polymeric porous scaffolds.[5] Hydrogels resemble natural extracellular matrices but inherently possess random pore and mesh sizes in the sub-micron regime, preventing control of cell adhesion and architecture.[6] Polymeric porous scaffolds provide tissue architecture, but the fabrication methods often produce pores of varying sizes and shapes[7–15] that complicate the mechanical effects of scaffold architecture on tissue cell behaviours. Constructing well-defined scaffold architecture consisting of identical microenvironment is therefore critical to understanding how the mechanical properties of microenvironments influence cellular behaviours.

Recent advances in computer-aided microfabrication techniques such as photolithographic patterning and layering,[16] direct writing,[17] and two-photon stereolithography[6] promote the fabrication of scaffolds with uniform pore size and controlled 3D interconnectivity. However, these methods are usually cost-prohibitive. A more cost-effective but time-consuming approach is based on an inverted colloidal crystal (ICC) in which large crystalline arrays of colloidal spheres are created, scaffold materials such as polyacrylamide or chitosan are deposited, and finally the colloidal spheres are removed.[18–20] The uniformity in pore size and structure of ICC scaffold leads to a higher diffusion rate and a more uniform distribution of cells than its counterpart with non-uniform pores.[21]However, the range of solid fraction is limited due to the condition of colloidal crystal assembly, and the pore size depends on the availability of colloidal microspheres.

Here we demonstrate a foam-based scaffold fabrication for ICC structure that is fast, inexpensive, and easily tunable for pore size and porosity. This investigation represents an improvement of a previous fabrication workflow.[22] A monodisperse liquid foam containing scaffold material was first generated through a flow-focusing microfluidic device (Fig. 1A and B) in which the bubble size and air fraction were controlled by varying the liquid flow rate and the air pressure.[23] The collected liquid foam self-assembled in a crystalline order that congealed into a solid foam with closed pores, which subsequently changed to the open-pore solid foam following degassing (Fig. 1C). Finally, the open-pore solid foam was used as a cell culture scaffold by seeding cells inside the pores.

[a]*Institute of Biophysics, National Central University, Chung-li, 32001, Taiwan. E-mail: khlin@phys.sinica.edu.tw; Fax: +886-2-2788-9829; Tel: +886-2-2789-6763*
[b]*Department of Physics, National Taiwan University, Taipei, 106, Taiwan*
[c]*Institute of Physics and Research Centers for Applied Sciences, Academia Sinica, Taipei, 115, Taiwan*
[d]*Department of Biology, University of North Carolina at Chapel Hill, Chapel Hill, NC, 27599, USA*
[e]*Instituto Gulbenkian de Ciencia, Cell Cycle Regulation Laboratory, Oeiras, Portugal*
[f]*Institute of Science and Technology, Vienna, Austria*
[g]*Instituto de Medicina Molecular, Lisbon, Portugal*

† Electronic supplementary information (ESI) available: Fig. S1 and S2 contain images of fibroblast morphologies after culture in 60 μm and 120 μm pores, respectively; Movie S1 shows that monodisperse bubbles are generated in a flow-focusing microfluidic device and self-organize into an ordered array of flowing lattice; Movies S2 and S6 contain the confocal images of MDCK and C2C12 cells in scaffolds; Movies S3–S5 are rendering movies of the fibroblasts attached in the pores shown in Fig. 5. See DOI: 10.1039/c1sm05371j

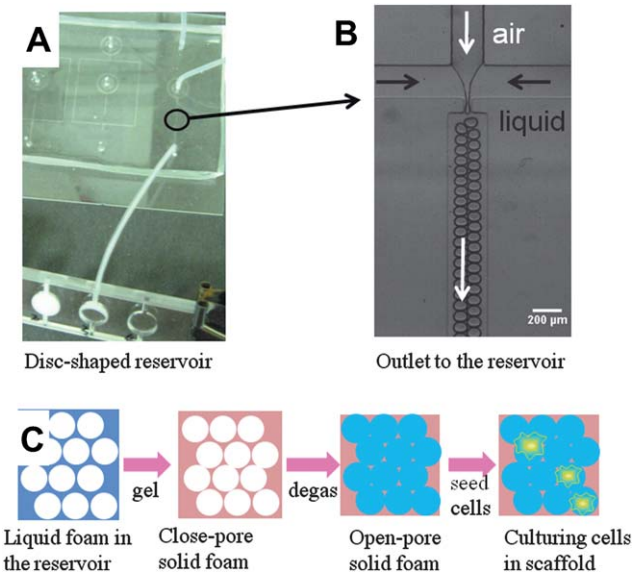

Fig. 1 Construction of 3D ordered cellular solids. (A) Photograph of the microfluidic device connected to the reservoir. (B) Microscopic snapshot of bubbles generated in a focusing flow at input liquid flow = 23 μl min^{-1} and air pressure = 20.5 psi. A video of this process is available as ESI, Movie S1†. (C) Monodisperse liquid foam self-assembled into crystalline order. The liquid foam was gelled into solid foam, at which point the bubbles became topologically closed cells (pores, distinct from biological cells) in the solid foam. Finally, the closed-pore solid foam was transformed to open-pore solid foam by degassing under vacuum while immersed in liquid crosslinking solution. The pressure difference between the inside and the outside of the pores was strong enough to rupture the film between the pores, allowing the crosslinking liquid to flow into the foam. As a result, the open-cell solid foam was suitable for use as a scaffold for 3D cell culture.

Usually the design principle for scaffolds is to mimic the structure of the native tissue environment. Here we invert the common paradigm and instead investigate how cells from different tissue types organize themselves in ordered cellular solids containing identical spherical pores. We found that cells preserve their original characteristics, and some exhibit new morphologies not observed on 2D substrates. Our findings shed light on 3D cell organization and promote systematic study of mechanical factors in tissue engineering and mechanobiology.

Materials and methods

Monodisperse foam generation

Chemicals, including gelatin, Pluronic® F127, glutaraldehyde, paraformaldehyde, glycine, and sodium borohydride, were purchased from Sigma-Aldrich and used without further purification. We used a planar flow-focusing microfluidic device made of polydimethylsiloxane[23] to generate monodisperse bubbles that self-assemble into highly ordered flowing lattices collected into disc-shape reservoirs through tubing. Foam production was not exposed to ambient air directly, improving foam stability. The liquid solution contained 7% gelatin and 1% Pluronic® F127 in deionized water and was pumped into the liquid inlet using the PhD 2000 syringe pump (Harvard Apparatus). The pressure of nitrogen mixed with perfluorohexane was monitored with a Heise PM pressure gauge. Typically, the liquid flow rate was 20–30 μl min^{-1} and the air pressure was 15–25 psi. The orifice where the air stream was focused by the liquid flow was 40 μm in diameter. During the process of bubble formation, the solution and the device were kept >40 °C so that the viscosity of the gelatin solution was below 14 mPa s. Bubbles were imaged in a Leica Z16 APO stereomicroscope with an ultrafast camera Miro3 (Vision Research) at an exposure time of 40 μs and 22 000 frames per second (ESI, Movie S1†). The air fraction of the liquid foam was determined by collecting the liquid foam in the known reservoir volume, V_r, and measuring the weight and the density of the liquid foam, W_l and D_l. The air fraction is $\phi_g = (V_r - W_l/D_l)/V_r$. Crosslinking and degassing did not substantially change the solid fraction, allowing us to use the air fraction as the porosity of the solid foam.

Open-cell solid foam fabrication

It took less than one minute to fill the reservoir, the disc-shaped scaffold mould with diameter 6 mm and height 1 mm, with liquid foam. The filled reservoir was placed at 4 °C for fast physical congealing to avoid coarsening. Critically, the temperature was kept above freezing to avoid the formation of tiny ice crystals inside the gelatin and the creation of microscopic pores that weaken the gelatin, make it very permeable to air, and reduce the effectiveness of pore bursting. The solid foam was next placed in crosslinking solution while being degassed in a vacuum of less than 20 Torr. The open-cell foam was later shaken at room temperature in 1 M glycine for 1 hour to quench the crosslinking reaction. Finally, the scaffold was shaken in phosphate-buffered saline for three successive one-hour washes, producing a scaffold ready for subsequent cell seeding.

Variations in crosslinking and quenching chemistry

Gelatin crosslinked by glutaraldehyde and quenched by glycine appears yellowish and emits strong autofluorescence, which can be reduced by substituting glutaraldehyde with paraformaldehyde or by quenching with sodium borohydride.[24] In the Madin–Darby canine kidney (MDCK) cell experiments, we used a mixture of 2% paraformaldehyde and 0.1% glutaraldehyde as a crosslinking solution to reduce background autofluorescence, allowing detection of the signal from the fluorescent protein. In the fibroblast experiments, we used 0.5% sodium borohydride to completely quench the autofluorescence, so the fibroblast cells could be segmented from the pores in the images. The fluorescence spectrum was measured with a fluorescence spectrophotometer (HORIBA Jobin Yvon). To improve scaffold visualization, the scaffolds were labelled with additional 0.01 mg ml^{-1} fluorescein isothiocyanate (Thermo) or Cy5-labeled *N*-hydroxysuccinimide ester (Amersham) dissolved in buffer containing 0.25 M sodium bicarbonate and 0.2 M NaCl [pH 9.5] for one hour.

Mechanical measurement of gel stiffness

The bulk mechanical stiffness of the crosslinked gelatin was measured with atomic force microscopy (AFM) using the Veeco Bioscope II. The force mode of the AFM was used to measure the indentation force and the indentation depth of the cantilever

(Bruker) on a thick layer of gelatin attached to a glass substrate. We fit the force–indentation curve by the Sneddon model[25] to calculate Young's modulus of gelatin gel, assuming a Poisson ratio of 0.5.

Cell culture

All reagents such as Dulbecco's Modified Eagle Medium (DMEM), calf bovine serum, fetal bovine serum (FBS), horse serum, and antibiotics (penicillin and streptomycin) were purchased from Gibco. Mouse 3T3 fibroblasts (ATCC CRL-1658) were cultured in DMEM supplemented with 10% calf bovine serum and 1% antibiotics. MDCK cells expressing the dsRed–E-cadherin proteins were kindly donated by James Nelson's group at Stanford University, Stanford, California, USA. These cells were cultured in DMEM supplemented with 10% FBS and 1% antibiotics, as were the mouse C2C12 myoblasts (ATCC CRL-1772). To induce myotube formation, 10% FBS in the culture medium was replaced with 10% horse serum as the differentiation medium. All cell cultures were maintained at 37 °C and 5% CO_2, and the medium was exchanged every other day. All cells were also cultured on 2D crosslinked gelatin gel, leading to morphologies that were similar to those observed on 2D cell culture dishes or glass as shown in ATCC website.[26]

On-scaffold cell culture

Prior to cell seeding, excess liquid in the scaffold was removed by pipetting. The cells were trypsinized and resuspended in culture medium at appropriate cell density (10^4 to 10^6 ml^{-1}). Ten to twenty microlitres of cell suspension were seeded into the scaffold and incubated at 37 °C and 5% CO_2 for 1 hour before immersing the scaffold in culture medium. Cell proliferation and viability were assessed with the Live/Dead Cell Viability Assay (Invitrogen). The death rate was less than 0.5%, and the cells proliferated well inside the scaffolds (Fig. 2). 3T3 and C2C12 cells were able to grow inside the scaffold for more than one month. MDCK cells became necrotic when they were overconfluent in the scaffold. In most of the experiments presented here, the cells were fixed for immunostaining after one day of culture in the scaffold. To observe myotube formation, cells were cultured in differentiation medium for more than ten days, and the medium was replaced every other day.

Cell staining and imaging

The cells were fixed in 4% paraformaldehyde and 0.1% Triton X in phosphate-buffered saline for 15 minutes at room temperature. The F-actin and nuclei of 3T3 and C2C12 cells were stained with 33 nM fluorescent phalloidin (Invitrogen) and 10 μg ml^{-1} 4′,6-diamidino-2-phenylindole (DAPI; Invitrogen), respectively, according to the manufacturer's instructions, and were imaged with an LSM 510 confocal microscope (Zeiss). MDCK cells were immunostained with a 1 : 100 dilution of mouse monoclonal anti-canine-GP135,[27] a gift from James Nelson's group, and 15 μg ml^{-1} Cy5-conjugated goat anti-mouse antibody (Jackson ImmunoResearch Lab) in addition to nuclear labelling with DAPI. MDCK cells were imaged with a FluoView FV1000 microscope (Olympus) and others were imaged with a Zeiss LSM510 microscope. Unless otherwise specified, all images were taken with 63× glycerol-immersion objectives. Images of the large area scan with a 10× objective were imaged by a spinning disc confocal CSU22 (Yokogawa) controlled by Metamorph 7.7.2. The images were processed with Imaris version 7.1 (Bitplane); the operations were adjusting contrast and brightness and smoothing with a Gaussian kernel. The reconstructed images were processed with "surface objective" function in Imaris. The pore size measurement was performed in ImageJ version 1.44 (NIH) and more than 50 pores were measured for each sample.

Results and discussion

Characterization of gelatin scaffolds

Here we used gelatin as a scaffold material, a modification that offers several advantages over previous fabrication methods. Gelatin is a denatured collagen on which adherent cells proliferate well; it can be physically gelled by quickly and uniformly lowering the temperature throughout the sample before the liquid foam coarsens, leading to a large crystalline array in the solid foam (Fig. 3A and B). The porosity of the scaffold is also tunable over a wide range (Fig. 3C and D). The pores are highly monodisperse over a large crystalline domain at the size range of millimetres. The polydispersity is less than 4% within a single domain of the crystalline foam. For these studies, the typical scaffold pore size ranged from 60 to 90 μm, the air fraction was ~60%, and the interconnected pore size was ~25 μm.

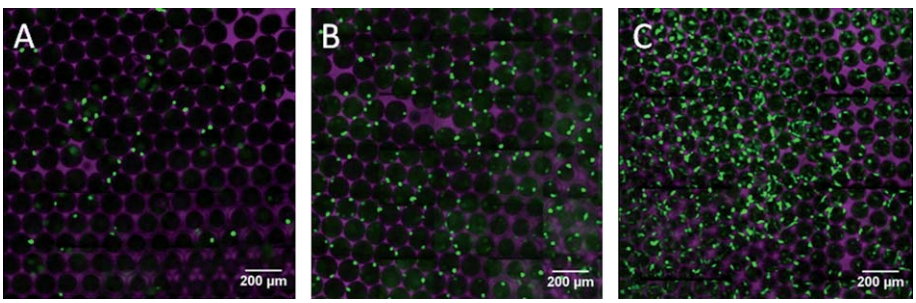

Fig. 2 Confocal microscopy of fibroblast cells taken: (A) 2, (B) 7, and (C) 9 days after cell seeding on gelatin foam scaffolds (purple). Images were taken with a 10× air objective and stitched together using the scanslide function of Metamorph. Live cells appear in green following staining with the Live/Dead Cell Viability Assay.

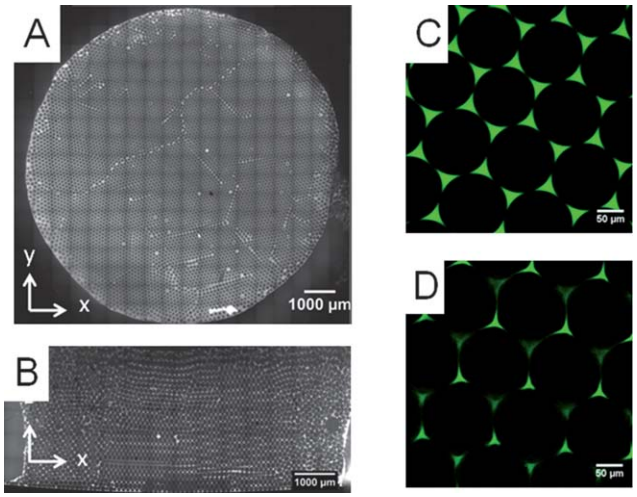

Fig. 3 An optical micrograph of a gelatin scaffold from the top (A) and the side (B) reveals a large array of uniform pores in crystalline order, with some point defects and dislocation lines. Images were taken with a 10× air objective and stitched together using the scanslide function of Metamorph 7.7.2. Confocal images show that the scaffolds with 65 μm have 56% porosity (C) and 86% porosity (D).

Physical gelation was reversible when the temperature was raised. The solid foam was further chemically crosslinked by glutaraldehyde and paraformaldehyde, then quenched to remove unreacted aldehyde groups, thereby making it compatible with living cells.[28] Crosslinking affects both the mechanical and optical properties of the scaffold. Glutaraldehyde-crosslinked gelatin emits strong autofluorescence, which can be reduced by substituting paraformaldehyde for glutaraldehyde. Using AFM, we measured the mechanical stiffnesses of the bulk gelatin as 420 000 Pa for the glutaraldehyde-crosslinked gelatin and 120 000 Pa for the paraformaldehyde-crosslinked gelatin. However, the paraformaldehyde crosslinking was reversible, and thus a mixture of glutaraldehyde and paraformaldehyde resulted in reliable mechanical integrity over time and lower autofluorescence. Although we used several crosslinking protocols, we did not detect substantial morphological changes in cells cultured on scaffolds crosslinked with different solutions.

Morphology and organization of tissue cells in the scaffolds

We tested the versatility of the 3D scaffolds for growing different cell types in uniform spherical pores. We assayed the morphology, physiology, and function of three distinct cell lines grown in these scaffolds: MDCK cells are derived from canine kidney epithelial cells, 3T3 fibroblast cells stem from mouse connective tissue, and C2C12 skeletal myoblast cells arise from mouse muscle tissue.

Epithelial tubes form elaborate networks in many organs to carry liquids containing nutrients, wastes, and other materials for exchange with the outside environment. To carry out directional transport, epithelial cells must acquire apicobasal polarity, establishing different structural and functional domains in a top domain (apical membrane) and a bottom domain (basolateral membrane) in the cell. Many epithelial cells, including MDCK cells, differentiate into a multicellular structure of polarized cells when grown in 3D gels of extracellular matrix materials such as collagen, forming spherical cysts characterized by a hollow lumen surrounded by a monolayer of polarized cells.[29] When we seeded MDCK cells at high density (>5 × 10^5 cells per ml) into scaffolds with preformed spherical pores, we found that within one day the MDCK cells organized into a confluent layer that conformed to the surface of the pores (Fig. 4). Similar to the conventional cyst structure (closed hollow spheres) adopted by cells grown in collagen gels, these MDCK cells formed spheres of cells that joined into both closed structures and open, interconnected structures. Confocal microscopy revealed the polarized nature of cells in the pores, another important characteristic of cysts. The apical surface of MDCK cells (green in Fig. 4) did not contact other cells or the scaffold, while the basolateral surface, which normally faces neighbouring cells and the substratum, was in contact with cells or substrate (red in Fig. 4), consistent with the polarity of MDCK cell sheets grown on 2D substrates.[30] Some cells aggregated (Fig. 4), exhibiting polarity consistent with the apical surface facing toward the free luminal surface.[31]

Fibroblasts, the most common cell type found in animal connective tissue contributes to synthesis and organization of the extracellular matrix. The surrounding microenvironment exerts a strong effect on fibroblast morphology; for example, fibroblasts spread thinly like a pan-fried egg on a hard surface, but elongate into spindle morphology when cultured in a 3D gel.[32,33] When 3T3 fibroblasts were grown onto the scaffolds, the cells adopted a diverse set of morphologies (Fig. 5). To better visualize a single cell in a pore, the cells were seeded at lower density (~5 × 10^4 cells per ml) and fixed after one day. Some cells spread onto the scaffold wall with most of the cell body on the wall

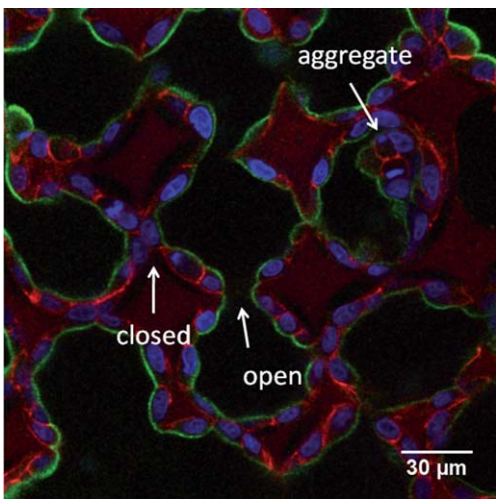

Fig. 4 MDCK epithelial cells form cyst-like confluent monolayers when grown in a scaffold with pores 70 μm in diameter. Nuclei (blue) were stained with DAPI. Apical membranes (green) were labelled with an antibody against GP135, an apical antigen.[27] Basolateral domains (bright red) are marked with E-cadherin tagged with ds-Red proteins. This scaffold was weakly autofluorescent (maroon), as it was crosslinked with a mixture of glutaraldehyde and paraformaldehyde. The arrows indicate several possible topological scenarios besides the confluent monolayer on the wall for MDCK cells: closed and open "cysts" at the pores as well as aggregates. The 3D confocal movie of these cells is available as ESI, Movie S2†.

("stickers;" Fig. 5A), while others appeared to straddle over scaffold pores and usually exhibited a spindle shape, using long pseudopodia to attach to opposite sides of the pore such that the body appeared to be bipolar symmetric and stretched ~180° ("stretchers;" Fig. 5B). Some cells were also observed to "squat" on the pore wall with short pseudopodia (Fig. 5C). The morphologies of other cells were intermediate in this cell-shape spectrum.

Stretchers were the most distinct morphological fibroblast type observed in this experiment. At a pore size of 65 μm, nearly 34% of cells were stretchers (11/34 examined cells; ESI, Fig. S1†), with most of the cells extending across the pore diameter. Larger pore sizes led to fewer squatters and more 2D-like "sticker" cells; at a pore size of 120 μm, the average extension of the stretcher cells which was defined as the end-to-end distance of the cell body was about 87 μm, much less than the pore diameter (ESI, Fig. S2†). In addition, fibroblast cells often resided within a pore without crossing to neighbouring pores; only at smaller pore sizes (40 μm) were cells stretched over two pores orthogonal to the wall of the interconnected pore (Fig. 5D). Interestingly, we also observed a partial cell body protruding to a neighbouring pore while the body was parallel to the wall of the interconnected pore at a larger pore size of 120 μm (Fig. 5E). It has been shown that there is a critical length and angle for cell protuberance over ridges or grooves[34] because cytoskeletal tension is inhibited at high substrate curvature.[35,36] We did not observe distinct stress fibres (thick, bundled actin filaments spanning the cell) in cells grown on the curved surfaces of the pores. While it was possible that the resolution of the confocal microscope was insufficient to resolve actin bundles distributed in 3D, cells resident on the flat section of the scaffolds exhibited thick stress fibres similar to cells resident on a flat glass substrate (data not shown). Taken together, we observed morphologies of 3T3 fibroblasts cultured in spherical pores that were rich and dependent on pore size.

C2C12, a myogenic cell line derived from mouse skeletal muscles, retains the capacity to differentiate *in vitro* into fused, multinucleated fibres.[35–37] After only one day of culture of a high density of cells (>5 × 10^5 cells per ml) seeded in the scaffolds, and prior to the addition of differentiation medium, a subset of the C2C12 cells grew on the curved pore surfaces, while other cells stretched into a line by forming strong contacts with cells in neighbouring pores (Fig. 6A). Lines of cells often grew along the

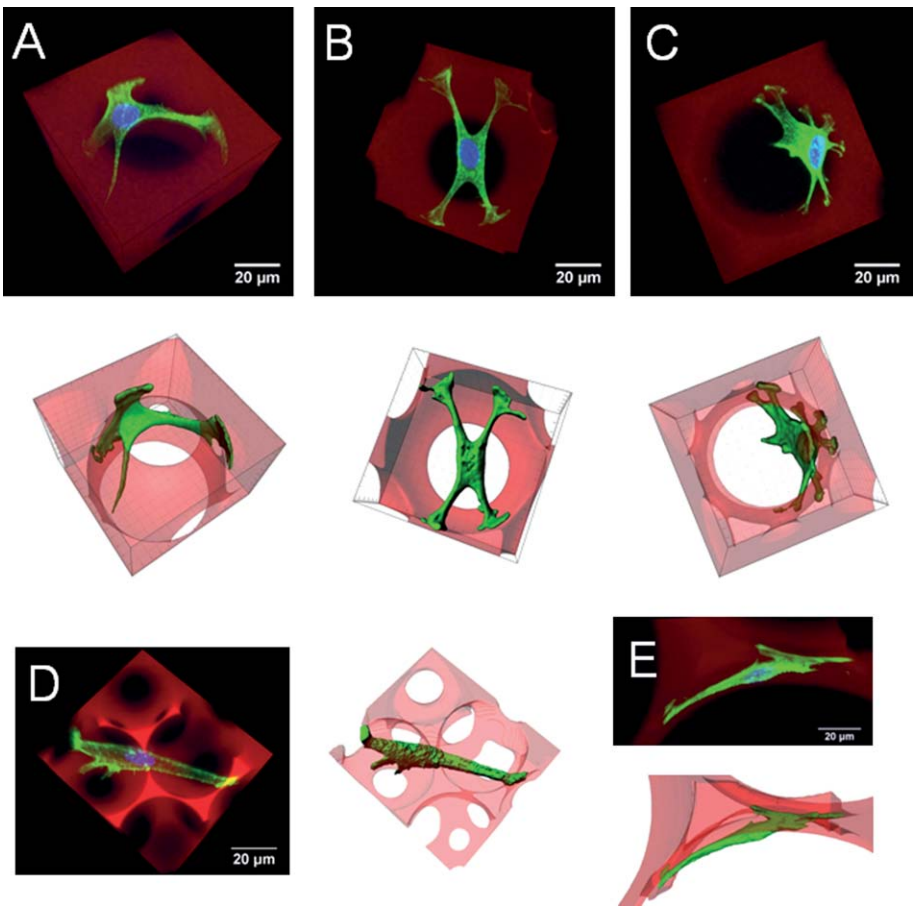

Fig. 5 3D-rendered (top) and reconstructed (bottom) images of the diverse morphologies exhibited by fibroblasts grown on a scaffold with 65 μm pores. Nuclei were stained with DAPI (blue), actin was stained with phalloidin (green), and the scaffold was labelled with fluorescein (red). The rendered images (top) were created by maximum intensity projection and the reconstructed images (below) were created by extracting the isosurfaces of the cell bodies and scaffolds from the intensities of the green and red channels, respectively. (A) Most of the cell body is spread on the wall of the spherical pore. (B) The cell straddles the pore with long legs. (C) The cell body is supported away from the wall by many small pseudopods. (D) A spindle-like cell body stretches over two pores. (E) The cell protrusion spreads to the neighbouring pore. The cell body shows two opposite curvatures along the pores. Rendered confocal images for panels (A–C) are available as ESI, Movies S3–5†, respectively.

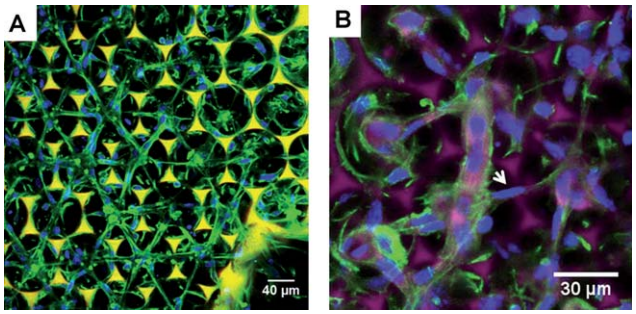

Fig. 6 C2C12 cells cultured in scaffolds with uniform pores adopted distinct morphologies before (A) and after (B) exposure to differentiation medium. (A) An asterisk pattern formed after only one day of growth in a scaffold with 85 μm pores (yellow). This image was taken with a 20× air objective. (B) Following exposure to differentiation medium for more than one month, a myotube (arrow) appeared in the culture of C2C12 cells resident on a scaffold with pores 60 μm in diameter (purple). Multiple nuclei (blue) were visible within the thick tube, evidence of myotube fusion. For both images, actin was stained with phalloidin (green) and nuclei were stained with DAPI (blue). Original confocal images for panel (A) are available as ESI, Movie S6†.

Table 1 Summary of morphological characteristics of tissue cell types cultured in the foam scaffold

Cell type	Characteristic morphology
Epithelial cells	Hollow sphere
Connective tissue cells	Diverse—spindle, spread, squatter, *etc.*
Muscle cells	Line

crystalline structure of the scaffold and exhibited a striking aster pattern (Fig. 6A), suggesting that the scaffold itself may initiate the differentiation process in C2C12 cells. In order to induce myotube formation, we exchanged the culture medium for differentiation medium after the linear patterns formed. We observed cells fused inside the scaffold after culturing in differentiation medium for more than 10 days, and a thick fused myotube with multiple nuclei appeared after culture with differentiation medium for more than one month (Fig. 6B). Despite the spherical shape of the scaffold pores, the C2C12 cells—which are tubular in the natural setting of the animal body—preserved and exhibited underlying physiological characteristics consistent with observations of their growth in 2D culture.

Conclusions

The scaffolds currently in use in tissue engineering investigations are highly diversified in terms of structure and materials, making systematic studies difficult. An increasing number of studies[21,36,38,39] have employed scaffolds with ICC structures to study 3D cell migration and applications for tissue engineering. Here we have demonstrated a simple, fast, and high-throughput method to produce scaffolds of similar structure that are uniform in pore size. Our approach is lower in cost and faster than the current ICC method[18] and allows the easy tuning in the pore size and the solid fraction. Additionally, this method is compatible with many hydrogels unlike the traditional gas foaming method.[12] Our novel scaffolds provide an ideal culture model because each pore represents a nearly identical mechanical microenvironment.

Table 1 summarizes the cell morphology in the scaffolds: confluent epithelial cells formed cyst-like polarized epithelial cell sheets comprised of spherical shells of cells (Fig. 4), fibroblasts exhibited a diverse set of morphologies (Fig. 5), and myoblasts contacted each other in a linear fashion and fused into a clearly recognizable myotube (Fig. 6). Though the foam scaffolds do not resemble the extracellular matrix of native tissues for many cell types, the cells still preserve their characteristic morphologies in the foam scaffolds. Our observation suggests that the scaffold simply positions the cells in 3D and the organization of the cells depends on the intrinsic characteristic of cell-matrix and cell-cell interactions.

For future study, primary cells grown in these scaffolds can be trypsinized and collected for downstream analysis, including gene expression analysis. We are currently taking advantage of these methodological strengths to investigate the biochemical response of cellular behaviours in pores of various sizes; we anticipate that the length scale of a pore is relevant for 2D *versus* 3D cell culture. Uniform and ordered cellular solids will also allow us to determine the mechanical properties of the struts or walls around the pores, knowledge that is crucial to understanding how cells respond to stiffness in 3D microenvironments.[40,41] Patterned 2D substrates have been shown to be useful for high-throughput cell arrays,[42] studies of 2D cell–matrix interactions,[43] and contact guidance for cell growth.[44] This 3D foam scaffold provides a suitable platform for generating periodic patterns in 3D and potentially can be used for high-throughput cell assays and for studying 3D cell–matrix interactions.

Acknowledgements

We thank A-jay Lin, Hsiang-haw Ning, Meng-ting Chung, Wan-hsin Chang, and Yen-liang Liu for their participation in developing gelatin scaffolds. We also thank the instructors, especially KC Huang, Wallace Marshall, and Dan Fletcher, and participants in the 2010 Physiology Course at the Marine Biological Laboratory for helpful discussion on image processing and AFM measurements. Nicolas Borghi and James Nelson from Stanford University provided MDCK cells, antibodies, and valuable discussion on MDCK-related work. Shu-chen Shen from the Academia Sinica imaging center helped in acquiring the confocal images. Tiffany Vora provided valuable discussion on the manuscript. We had productive discussions with Jungwoo Lee comparing our approach to other scaffold fabrication methods. This work was supported by Academia Sinica Nano-Bio funding, the National Science Council (99-2112-M-001), and the Penn MRSEC (DMR-0520020) LRSM-Sinica collaboration.

Notes and references

1 K. Bhadriraju and C. S. Chen, *Drug Discovery Today*, 2002, **7**, 612–620.
2 A. J. Engler, S. Sen, H. L. Sweeney and D. E. Discher, *Cell*, 2006, **126**, 677–689.
3 C. M. Nelson and M. J. Bissell, *Annu. Rev. Cell Dev. Biol.*, 2006, **22**, 287–309.

4 L. G. Griffith and M. A. Swartz, *Nat. Rev. Mol. Cell Biol.*, 2006, **7**, 211–224.
5 J. Lee, M. J. Cuddihy and N. A. Kotov, *Tissue Eng., Part B: Rev.*, 2008, **14**, 61–86.
6 P. Tayalia, C. R. Mendonca, T. Baldacchini, D. J. Mooney and E. Mazur, *Adv. Mater.*, 2008, **20**, 4494–4498.
7 R. Y. Zhang and P. X. Ma, *J. Biomed. Mater. Res.*, 1999, **44**, 446–455.
8 H. Yoshimoto, Y. M. Shin, H. Terai and J. P. Vacanti, *Biomaterials*, 2003, **24**, 2077–2082.
9 K. Whang, C. H. Thomas, K. E. Healy and G. Nuber, *Polymer*, 1995, **36**, 837–842.
10 M. C. Wake, P. K. Gupta and A. G. Mikos, *Cell Transplant.*, 1996, **5**, 465–473.
11 R. C. Thomson, M. J. Yaszemski, J. M. Powers and A. G. Mikos, *J. Biomater. Sci., Polym. Ed.*, 1995, **7**, 23–38.
12 D. J. Mooney, D. F. Baldwin, N. P. Suh, L. P. Vacanti and R. Langer, *Biomaterials*, 1996, **17**, 1417–1422.
13 A. G. Mikos, G. Sarakinos, S. M. Leite, J. P. Vacanti and R. Langer, *Biomaterials*, 1993, **14**, 323–330.
14 P. Eiselt, J. Yeh, R. K. Latvala, L. D. Shea and D. J. Mooney, *Biomaterials*, 2000, **21**, 1921–1927.
15 A. Barbetta, A. Gumiero, R. Pecci, R. Bedini and M. Dentini, *Biomacromolecules*, 2009, **10**, 3188–3192.
16 D. Gallego, N. Ferrell, Y. Sun and D. J. Hansford, *Mater. Sci. Eng., C*, 2008, **28**, 353–358.
17 J. L. Simon, S. Michna, J. A. Lewis, E. D. Rekow, V. P. Thompson, J. E. Smay, A. Yampolsky, J. R. Parsons and J. L. Ricci, *J. Biomed. Mater. Res., Part A*, 2007, **83A**, 747–758.
18 N. A. Kotov, Y. F. Liu, S. P. Wang, C. Cumming, M. Eghtedari, G. Vargas, M. Motamedi, J. Nichols and J. Cortiella, *Langmuir*, 2004, **20**, 7887–7892.
19 A. N. Stachowiak, A. Bershteyn, E. Tzatzalos and D. J. Irvine, *Adv. Mater.*, 2005, **17**, 399.
20 S. W. Choi, J. W. Xie and Y. N. Xia, *Adv. Mater.*, 2009, **21**, 2997–3001.
21 S. W. Choi, Y. Zhang and Y. N. Xia, *Langmuir*, 2010, **26**, 19001–19006.
22 K. Y. Chung, N. C. Mishra, C. C. Wang, F. H. Lin and K. H. Lin, *Biomicrofluidics*, 2009, **3**, 022403.
23 P. Garstecki, I. Gitlin, W. DiLuzio, G. M. Whitesides, E. Kumacheva and H. A. Stone, *Appl. Phys. Lett.*, 2004, **85**, 2649–2651.
24 G. T. Hermanson, *Bioconjugate Technique*, Academic Press, San Diego, 1996.
25 M. T. Frey, A. Engler, D. E. Discher, J. Lee and Y. L. Wang, in *Cell Mechanics*, Elsevier Academic Press Inc, San Diego, 2007, vol. 83, pp. 47–65.
26 http://www.atcc.org/Attachments/1766.jpg, (MDCK), http://www.atcc.org/Attachments/1776.jpg, (3T3), http://www.atcc.org/Attachments/1834.jpg, (C2C12).
27 G. K. Ojakian and R. Schwimmer, *J. Cell Biol.*, 1988, **107**, 2377–2387.
28 E. Khor, *Biomaterials*, 1997, **18**, 95–105.
29 N. Elia and J. Lippincott-Schwartz, *Culturing MDCK Cells in Three Dimensions for Analyzing Intracellular Dynamics*, John Wiley & Sons, Inc., 2001.
30 L. E. O'Brien, M. M. P. Zegers and K. E. Mostov, *Nat. Rev. Mol. Cell Biol.*, 2002, **3**, 531–537.
31 A. Z. Wang, J. C. Wang, G. K. Ojakian and W. J. Nelson, *Am. J. Physiol.*, 1994, **267**, C473–C481.
32 P. Weiss, *Rev. Mod. Phys.*, 1959, **31**, 11–20.
33 T. Elsdale and J. Bard, *J. Cell Biol.*, 1972, **54**, 626–637.
34 P. M. Stevenson and A. M. Donald, *Langmuir*, 2009, **25**, 367–376.
35 J. A. Sanz-Herrera, P. Moreo, J. M. Garcia-Aznar and M. Doblare, *Biomaterials*, 2009, **30**, 6674–6686.
36 S. R. Peyton, Z. I. Kalcioglu, J. C. Cohen, A. P. Runkle, K. J. Van Vliet, D. A. Lauffenburger and L. G. Griffith, *Biotechnol. Bioeng.*, 2011, **108**, 1181–1193.
37 H. M. Blau, G. K. Pavlath, E. C. Hardeman, C. P. Chiu, L. Silberstein, S. G. Webster, S. C. Miller and C. Webster, *Science*, 1985, **230**, 758–766.
38 J. Lee, M. J. Cuddihy, G. M. Cater and N. A. Kotov, *Biomaterials*, 2009, **30**, 4687–4694.
39 A. N. Stachowiak and D. J. Irvine, *J. Biomed. Mater. Res., Part A*, 2008, **85A**, 815–828.
40 B. A. Harley, J. H. Leung, E. Silva and L. J. Gibson, *Acta Biomater.*, 2007, **3**, 463–474.
41 S. Nemir and J. L. West, *Ann. Biomed. Eng.*, 2010, **38**, 2–20.
42 V. I. Chin, P. Taupin, S. Sanga, J. Scheel, F. H. Gage and S. N. Bhatia, *Biotechnol. Bioeng.*, 2004, **88**, 399–415.
43 N. Borghi, M. Lowndes, V. Maruthamuthu, M. L. Gardel and W. J. Nelson, *Proc. Natl. Acad. Sci. U. S. A.*, 2010, **107**, 13324–13329.
44 M. D. Guillemette, B. Cui, E. Roy, R. Gauvin, C. J. Giasson, M. B. Esch, P. Carrier, A. Deschambeault, M. Dumoulin, M. Toner, L. Germain, T. Veres and F. A. Auger, *Integr. Biol.*, 2009, **1**, 196–204.

